bioRxiv preprint doi: https://doi.org/10.1101/2021.07.07.451494; this version posted July 9, 2021. The copyright holder for this preprint (which was not certified by peer review) is the author/funder. All rights reserved. No reuse allowed without permission.

Directional Cell Migration Guided by a Strain Gradient

Feiyu Yang[1], *Yubing Sun*[1,2,3*]

[1]Department of Mechanical and Industrial Engineering, University of Massachusetts Amherst, Amherst, Massachusetts 01003, USA

[2]Department of Biomedical Engineering, University of Massachusetts Amherst, Amherst, Massachusetts 01003, USA

[3]Department of Chemical Engineering, University of Massachusetts Amherst, Amherst, Massachusetts 01003, USA

*Correspondence to ybsun@umass.edu (Yubing Sun)

KEYWORDS

Single cell migration, cell stretching device, strain gradient, focal adhesion, tensotaxis, mechanotransduction.

bioRxiv preprint doi: https://doi.org/10.1101/2021.07.07.451494; this version posted July 9, 2021. The copyright holder for this preprint (which was not certified by peer review) is the author/funder. All rights reserved. No reuse allowed without permission.

ABSTRACT

Strain gradients, the percentage of the deformation changed across a continuous field by applying forces, have been observed in developing tissues due to the inherent heterogeneity of the mechanical properties. The directional movement of cells are essential for proper cell localization, and it is well-established that cells establish directional migration in responses to gradients of chemicals, rigidity, density of extracellular matrices, and topography of substrates. However, it is unclear whether strain gradients imposed on cells due to tissue growth are sufficient to drive directional cell migration. In this work, we develop a programmable uniaxial cell stretch device coupled with geometrical constraints to create controllable strain gradients on cells. We demonstrate that single rat embryonic fibroblasts (REFs) respond to very small strain gradients. In a gradient level of 4% per mm, 60%-70% of the REFs prefer to migrate towards the lower strain side in both the static and the 0.1 Hz cyclic stretch conditions. We confirm that such responses to strain gradient is distinct from durotaxis or haptotaxis. Moreover, by using the YFP-Paxillin reporter, we discover that the directional migration of the cells is initiated by increasing focal adhesion contact areas and higher rate of protrusion formation in the lower strain side of the cell. Together, in this work we establish strain gradient as a novel cue to regulate directional cell migration and may provide new insights in development and tissue repairs.

bioRxiv preprint doi: https://doi.org/10.1101/2021.07.07.451494; this version posted July 9, 2021. The copyright holder for this preprint (which was not certified by peer review) is the author/funder. All rights reserved. No reuse allowed without permission.

INTRODUCTION

Cells are also constantly exposed to mechanical strain due to tissue growth (1), fluid flow (2), muscle contraction (3), etc. Numerous in vitro and in vivo studies support that mechanical strain is critically involved in various developmental and physiological processes, including the maturation of cardiac tissues (4), lung remodeling, and epithelial regeneration (5). While the majority of the research focuses on the cellular responses to uniform strains, it has been observed in Xenopus ectoderm tissues that cells migrate along a strain gradient when subjected to concentrated loading, a process termed as "tensotaxis" (6). This phenomenon is drastically different from what has been repeatedly reported in the literature, which demonstrates that cells reorientated perpendicular to the principal strain direction (7-9). In the context of early embryo development, the heterogeneity of tissue stiffness has been observed in embryos (10, 11), and directional migration of mesenchymal-like cells has been found during early embryo development (12). These evidence suggest the existence of a strain gradient in developing embryos, which may guide the directional migration of individual cells (13).

The directional cell migration can be guided by both biochemical and biomechanical cues in cell microenvironment, including gradients of chemical exposure (chemotaxis) (14), substrate bonded proteins (haptotaxis) (15, 16), substrate topography (topotaxis) (17), and the stiffness variations on the extracellular matrices (durotaxis) (18). Tensotaxis has yet been established as a biomechanical cue to guide directional cell migration, partially due to the difficulty to generate a controllable and physiologically relevant strain gradient (1-100% mm^{-1}) (19), and more importantly, the challenge to distinguish durotaxis and tensotaxis, as substrate stiffness

bioRxiv preprint doi: https://doi.org/10.1101/2021.07.07.451494; this version posted July 9, 2021. The copyright holder for this preprint (which was not certified by peer review) is the author/funder. All rights reserved. No reuse allowed without permission.

changes with strain due to nonlinear material responses (20, 21). Thus, tensotaxis and durotaxis are often used interchangeably, referring to the mechano-responsiveness of cells (22), while cells may utilize completely different mechanisms to sense strains and substrate stiffness.

Non-uniform strain fields have been achieved using various approaches (23-27). In those works, it is consistently reported that cell reorientation is a function of strain magnitude and cells tend to avoid strain gradient and align perpendicular to the principal strain directions. Surprisingly, the tensotaxis behaviors have not been observed, likely due to suboptimal cell stretching protocol, strain magnitude, and lack of consistency in strain gradient.

In this work, we developed a novel strain gradient generation device by introducing void regions with defined geometries to a membrane. Arduino microcontroller was used to precisely control the frequency and magnitude of uniaxial stretch with a servomotor. Using this device, we examined whether fibroblasts, which underwent constant stretches in vivo (28), respond to strain gradients directly. We found that under static stretch, >60% of rat embryonic fibroblasts (REFs) migrated towards the lower strain direction in a gradient level of 4% mm^{-1}. Using pre-stretched membranes, we showed that the strain gradient induced directional cell migration was not due to durotaxis. We further demonstrated that the dynamics of focal adhesion and formation of protrusions were responsible for the tensotaxis. Together, our study establishes tensotaxis as a novel biomechanical cue to guide the directional migration of cells.

RESULTS

bioRxiv preprint doi: https://doi.org/10.1101/2021.07.07.451494; this version posted July 9, 2021. The copyright holder for this preprint (which was not certified by peer review) is the author/funder. All rights reserved. No reuse allowed without permission.

Design and fabrication of the device for generating strain gradients

To study the effects of strain gradient on cell migration, it is essential to generate a controllable strain gradient to allow the migration of single cells in an optimal culture environment. Devices using microfluidic or vacuum to stretch cells can generate non-uniform strains. However, it is difficult to maintain a consistent uniform strain gradient (29, 30). On the other hand, some systems require the encapsulation of cells in a sealed configuration (31). It is difficult to maintain the oxygen, pH, and nutrition conditions at optimal levels for long-term cell culture, and the profusion flow may introduce undesired shear stress, causing unexpected cellular responses (32).

To address these issues, we design a new device for generating controllable strain gradients. This device was comprised of two primary components, the cell culture chamber and the control panel (**Fig. 1a**). In the control panel, a programmable servo motor attached with a rotational gear was fixed in the middle. Two translational gears were tightly jointed with the rotational gear (**Fig. 1b**). By controlling the rotational gear's motion on the servo motor, the translational gears were driven to perform a linear movement for uniaxial cell stretching. The strain gradients were generated by a double-layer membrane fixed at the end of the translational gears (**Fig. 1c**). The bottom layer is a silicone film (1/32 inch) with cut-out of desirable geometries produced by laser cutting. On the top of the silicone base, we plasma-bonded a layer of flat polydimethylsiloxane (PDMS) membrane, and the whole membrane was sandwiched between two glass slides at the end (**Fig. 1c**). The advantage of this design is that the strain gradient can be modulated by the geometry of the cut-out, which is independent of

bioRxiv preprint doi: https://doi.org/10.1101/2021.07.07.451494; this version posted July 9, 2021. The copyright holder for this preprint (which was not certified by peer review) is the author/funder. All rights reserved. No reuse allowed without permission.

the stretching magnitude. The assembly was mounted to the stretching device by clamped the two glass slides tightly with acrylic screws (**Fig. 1d**). To improve the live-cell imaging quality, during the experiment the cell stretch device was flipped upside down and the membrane was mounted onto the device from the opening below (**Fig. S1**). We then placed a 60 mm petri dish underneath and assembled the removable bottom to seal the cell culture chamber. At the start of each experiment, the membrane should be placed flat but not in a stretched status.

Characterization of the strain field

To establish the correlation between the cut-out geometry and the strain gradient, we first used finite element analysis (Ansys) to simulate the strain field under uniaxial stretching. We found that a graded and a uniform strain field were established on the cell culture regions for the triangle and the square designs, respectively (**Fig. 1e**). To validate the simulation result, we further sought to characterize the device by mapping the strain field experimentally. we applied the micro-contact printing technique to print small markers with equal distance across the cell culture surface to calculate the strain across the cell culture area (**Fig. S2**). Images were taken before and after applying the stretch, and the displacement of markers was tracked using ImageJ (**Fig. S2a**). The strain between two adjacent markers was calculated by dividing the change of distance by the initial distance (**Fig. S2b**). Consistent with the simulation results, we found that stretching the membrane with triangle cut-out by applying 15-degree rotation with the rotational gear led to strains between 12% to 18% across a horizontal distance of 1.5 mm, equivalent to a strain gradient of ~4% mm^{-1}, while a uniform 15% strain was found for the membrane with square cut-out by applying 20-degree rotation with the rotational gear (**Fig. 1f**).

bioRxiv preprint doi: https://doi.org/10.1101/2021.07.07.451494; this version posted July 9, 2021. The copyright holder for this preprint (which was not certified by peer review) is the author/funder. All rights reserved. No reuse allowed without permission.

As shown in **Fig. S3**, the sample-to-sample variation was very small, suggesting this approach could reproducibly generate controllable strain gradients. The detailed experiment procedures and simulations can be found in the Method section.

It is possible that after extended cell culture or cyclic stretching, the changes of the material properties of the membrane may influence the strain field. To evaluate the stability of the strain gradient under these experimental conditions, samples were calibrated first, submerged into 1× DPBS in a 37 °C incubator for 24 hrs, cyclic stretched at 0.1 Hz for 3 hours, and then were calibrated again. We found no significant changes in the strain field, suggesting that in our experimental conditions, the strain field remained stable.

REFs migrate directionally towards lower strain direction

We next investigated whether the migration of REFs could be influenced by the strain gradient. To avoid the haptotaxis effect caused by non-uniform ligand density due to the presence of strain gradient, we first stretched the membranes to desirable magnitude, coated the membrane with fibronectin for 1 hr, and then released the membrane to relaxed status. We then seeded single REFs on unstretched membranes with triangular and square cut-outs. After 15 hrs of culture, a static stretching was applied to the membrane using the same conditions as in **Fig. 1f,** so that the gradient and uniform conditions have a comparable average strain of 15%. The membranes were held at the stretched status for the next 6 to 8 hrs and cell migration trajectories were tracked using live-cell microscopy (**Fig. 2a, Video S1-S5**). To avoid the potential boundary effects, only the cells in the center of the cell culture area were tracked. To

bioRxiv preprint doi: https://doi.org/10.1101/2021.07.07.451494; this version posted July 9, 2021. The copyright holder for this preprint (which was not certified by peer review) is the author/funder. All rights reserved. No reuse allowed without permission.

minimize the influence of intercellular interactions, cells were seeded at a low density, and only samples with a total cell number of less than 170 cells were analyzed. Notably, only a few cells divided within the first 24 hours after cell seeding, and the cells that divided during the experiment period would not be tracked.

To quantify the directionality of the cell migration relative to the strain gradient direction, we set up local coordinates for each cell with the x-axis being the maximum gradient direction (**Fig. 2b**). We then connected the first and the last cell coordinate during the cell tracking period to calculate the migration angles. When the migration angle was between 90º to 270 º, the cells were considered migrating towards the lower strain direction. On the other hand, when the migration angle was between 0º to 90º or 270º to 360º, the cells were considered migrating towards the higher strain direction (**Fig. 2b**). For the uniform strain conditions, as no strain gradient was established, the x-axis was set to be along the stretch direction.

Histograms were plotted for visualizing cell migration direction preferences (**Fig. 2c**). We found a majority of cells (60%-70%) migrating towards the lower strain direction in the strain gradient group and the statistical significance was confirmed by the Rayleigh test. In contrast, in the uniform strain condition, there is no preference in the directionality of cell migration (**Fig. 2c**).

Tensotaxis is distinct from durotaxis

When the PDMS membranes were stretched, the strain gradient could potentially lead to a

bioRxiv preprint doi: https://doi.org/10.1101/2021.07.07.451494; this version posted July 9, 2021. The copyright holder for this preprint (which was not certified by peer review) is the author/funder. All rights reserved. No reuse allowed without permission.

variation of stiffness across the PDMS membrane due to the non-linear mechanical property of PDMS (33, 34). Therefore, durotaxis, a directional cell migration signal induced by stiffness gradient could potentially coexist with the tensotaxis. Moreover, micro-size fibrillar structures could be established on the PDMS membrane due to stretching as well, which might affect cell migration preferences (35). To exclude the influence of these factors, we first stretched the membrane and then coated the membrane with fibronectin to create a uniform ECM coating. We next seeded cells on the membrane and tracked the migration of the cells after 15 hrs of incubation (**Fig. 2d**). In this condition, cells would not be subjected to stretch, therefore not being exposed to the strain and the strain gradient, while the condition of the substrates was the same as the static strain gradient group shown in **Fig. 2c**. No significant preference of cell migration was found in this pre-stretched condition, suggesting that cells directly sense the strain gradient to the cell body, rather than substrate mechanical properties.

Cyclic stretching induces cell migration perpendicular to stretching direction

We next investigated whether cyclic stretching induced different migration patterns. Both membranes with triangle and square cut-out were cyclically stretched for the first 3 hours at 0.1 Hz, then was held at the stretched status for the next 3 hours. We found that interestingly, more cells migrated to the direction perpendicular to the strain gradient / stretching directions (migration angle close to 90º and 270º), compared to the static condition (**Fig. 2e**). This trend is more prominent for the uniform strain condition. However, under cyclic stretching conditions, we still observed a significantly high percentage of cells migrated towards the lower strain direction for the strain gradient condition (**Fig. 2e**). These data suggested that cell reorientation

bioRxiv preprint doi: https://doi.org/10.1101/2021.07.07.451494; this version posted July 9, 2021. The copyright holder for this preprint (which was not certified by peer review) is the author/funder. All rights reserved. No reuse allowed without permission.

to avoid strain gradients and tensotaxis are two independent, competing mechanisms to regulate directional cell migration upon stretching. This observation is further confirmed by the statistical analysis comparing the percentage of cells migrating towards smaller strain direction, which demonstrated that cells migrated along the strain gradient direction only in the presence of a strain gradient (**Fig. 2f**).

Quantifying tensotaxis using the forward migration index

We next evaluated the efficacy of the tensotaxis by quantifying the forward migration index ($FMI^{||}$) (36, 37), which was the ratio of the cell migration distance in the maximum gradient direction and the accumulated distance (**Fig. 2g**). When the $FMI^{||}$ was equal to 1 or -1, the cell migrated along or against the maximum gradient direction with no deviations, respectively. As such, a higher value of $FMI^{||}$ represents a higher efficacy of tensotaxis response. Consistent with the histograms, we found that both static and cyclic stretching of cell-seeded samples with strain gradient led to more cells with the $FMI^{||}$ closer to 1, with an average $FMI^{||}$ of 0.2 (**Fig. 2h,i**). In comparison, the pre-stretched condition led to an average $FMI^{||}$ closer to 0 (**Fig. 2h,i**). Notably, the $FMI^{||}$ for durotaxis of multiple cell types are smaller than 0.2 (38), suggesting that strain gradient is a potent cue to drive directional cell migration.

Strain magnitude regulates tensotaxis response rate

We next investigated how strain magnitude regulated the tensotaxis. We divided each strain gradient sample's cell culture area into two regions (**Fig. 3a**). Cells in Region 2 (R2) experienced a higher strain magnitude (15%-17%) comparing with those in Region 1 (R1, 13-

bioRxiv preprint doi: https://doi.org/10.1101/2021.07.07.451494; this version posted July 9, 2021. The copyright holder for this preprint (which was not certified by peer review) is the author/funder. All rights reserved. No reuse allowed without permission.

15%), and a similar gradient of 4% mm^{-1}. We compared the $FMI^{||}$ for cells in both regions under static stretching, cyclic stretching, and pre-stretch conditions. As shown in **Fig. 3b-c**, we found that in the static stretching group, the $FMI^{||}$ was significantly larger for the cells in R2 than R1 (**Fig. 3b-c**), suggesting a higher strain magnitude triggers a stronger tensotaxis response. No significant differences were found between the two regions in the cyclic stretching group, nor the pre-stretched control group. Together, these results suggest that while strain magnitude can regulate tensotaxis, the cyclic stretching induced cell reorientation may disrupt the cellular sensing of the strain magnitude.

Increasing focal adhesion formation and cell protrusion on the lower strain side of cells

We next investigated molecular mechanisms for the tensotaxis. As actin polymerization drive cell protrusion and the formation of new adhesion sites are the two most critical steps in cell locomotion (39), we sought to investigate the directionality of single-cell protrusion and focal adhesion dynamics under a strain gradient. The REF52 cell line we used has been transfected with a YFP-Paxillin reporter (40), and thus live-cell microscopy was used to evaluate the dynamics of paxillin containing focal adhesions. Cells cultured on membranes with triangle cut-out were imaged before and 20 mins after stretching (**Fig. 4a**).

To analyze the focal adhesion dynamics as a function of strain gradient, we divided each cell into two halves along the axis passing the center of the cell nucleus and perpendicular to the strain gradient direction (blue line in **Fig. 4a**). We used ImageJ to automatically identify each focal adhesion and quantified their sizes. After compensating for strain-gradient induced

bioRxiv preprint doi: https://doi.org/10.1101/2021.07.07.451494; this version posted July 9, 2021. The copyright holder for this preprint (which was not certified by peer review) is the author/funder. All rights reserved. No reuse allowed without permission.

artifacts (see Methods for details), we found that the total focal adhesion area increased significantly on the lower strain side while decreased on the higher strain side compared with the same region before stretching (**Fig. 4b**).

We next quantified the cell protrusion and retraction on the lower and higher strain sides. By tracing the cell boundaries before and after stretching, we found that within 20 mins after stretching, a significant protrusion could be found on the lower strain side of most cells analyzed, in contrast to the retraction on the higher strain side of cells (**Fig. 4c-d**). Sixteen out of seventeen cells were analyzed for both focal adhesion and protrusion. Ten in sixteen, i.e., 62.5% of cells, have a higher rate of protrusion formation and a relative increase of focal adhesion contact area at the lower strain direction at the same time., which conformed to the tensotaxis response rate shown in **Fig. 2c**. Together, these results suggest that protrusion and preferential formation of focal adhesions on the lower strain side of the cell may lead to the tensotaxis of cells.

DISCUSSION

Many tissues with anisotropic mechanical properties were subject to constant deformation during development and normal physiological activities. While the cell reorientation under strain and strain gradient has been well-studied, it is unclear whether such strain gradient also guides directional cell migration. This is particularly important to fully understand the principle of morphogenesis during development. In this work, we showed that fibroblasts are extremely sensitive to a small strain gradient (4% mm^{-1}) and migrate toward the lower strain direction

bioRxiv preprint doi: https://doi.org/10.1101/2021.07.07.451494; this version posted July 9, 2021. The copyright holder for this preprint (which was not certified by peer review) is the author/funder. All rights reserved. No reuse allowed without permission.

under static stretching. While cyclic stretching induced cell reorientation towards the direction perpendicular to cell stretching, we still observed an independent tendency for cell migration along the cell stretching direction toward the lower strain side. Our results also demonstrate that the tensotaxis of cells depends on the magnitude of strain and is initiated by strain-dependent focal adhesion formation and cell protrusion. Together, our data unambiguously establish the tensotaxis phenomenon of fibroblasts, which is distinct from durotaxis and haptotaxis.

The observation of the tensotaxis is allowed by our novel strain gradient generation device. Our approach allows a continuous strain gradient in mm scale for long-term cell migration tracking, distinct from the non-uniform strain field generated by applying concentrated forces. Compared to microfluidic-based and commercially available cell stretchers, our device is made of acrylics, silicone, and PDMS, all of which are low-cost and easy to manufacture, with the need of using special microfabrication tools. As the strain gradient can be tuned by changing the geometry of the cut-out without altering stretching parameters, the strain gradient and stretching magnitude, frequency, and strain rate can be controlled independently. Also, our device provides a culture condition similar to a regular culture flask for sensitive cell types. No shear forces caused by the flow of media or air were introduced in the system. Future works shall focus on modifying the device to study how strain gradient and other strain parameters synergistically regulate cell migration and other cell functions such as stem cell differentiation.

Our experiment (**Fig. 2d**) clearly demonstrated that tensotaxis is distinct from durotaxis and

bioRxiv preprint doi: https://doi.org/10.1101/2021.07.07.451494; this version posted July 9, 2021. The copyright holder for this preprint (which was not certified by peer review) is the author/funder. All rights reserved. No reuse allowed without permission.

haptotaxis. No preference in cell migration directionality was found when the membrane was pre-stretched and coated uniformly with fibronectin. This is likely due to the range of substrate stiffness cells can sense is very narrow (10^{-1}-10^{2} kPa), and durotaxis was generally investigated using soft hydrogel with a low rigidity (2 kPa – 7 kPa) (18) . In contrast, the Young's modulus for the PDMS membrane was reported to be over 1MPa, on which durotaxis is not prominent (34, 38). It has been established that cells utilize mechanosensitive focal adhesions (41, 42) and filopodia structures (43), and contractile machinery (44). Our results in Fig. 4 also show that the focal adhesions are also sensitive to strain and the stability and/or formation of new focal adhesions are preferred on regions with lower strain, which may facilitate the protrusion of cells towards lower strain direction. One possible explanation is the catch-slip bond-like behaviors observed in focal adhesions (40). Smaller strain may lead to a force-dependent stabilization of focal adhesions ("catch"), while larger strain may lead to the dissociation of focal adhesions (slip). This can also explain the observation that tensotaxis is more prominent in regions with smaller average strain, as the strain above a threshold will only lead to dissociation of focal adhesions (**Fig. 3**). These results suggest that tensotaxis may crosstalk with durotaxis to direct cell migration direction.

In conclusion, by generating a controllable strain gradient on cells, we demonstrated cells directly respond to a strain gradient and migrate directionally to the direction with lower strain. This mechanosensitive behavior, termed tensotaxis, is distinct from durotaxis or haptotaxis, and depends on the magnitude of the strain applied to the cells. Subcellular analysis revealed that lower strain increases the levels of focal adhesions and facilitates cell spreading. Together,

bioRxiv preprint doi: https://doi.org/10.1101/2021.07.07.451494; this version posted July 9, 2021. The copyright holder for this preprint (which was not certified by peer review) is the author/funder. All rights reserved. No reuse allowed without permission.

we establish the strain gradient as a mechanical cue to guide the directional migration of single cells and provide insights into the mechanisms of tissue remodeling and morphogenesis.

METHODS

Device and cell culture sample fabrication

Parts of the cell stretching device were printed with a laser cutter (40 Watt Epilog Mini 18 × 12) using the acrylic sheet (**Fig. 1a**), and assembled with screws and sealed with PDMS. In the control panel, a programmable servomotor (DS3218, Annimos) attached with a rotational gear was fixed in the middle. The Arduino Uno microcontroller was adopted to control the servomotor. Two translational gears were properly joined with the rotational gear on two sides, which were designed to connect the cell culture chamber with the control panel (**Fig. 1b**). Two small openings in between allowed the translational gears to extend into the cell culture chamber. We wrapped parafilm (PM-996, Bemis) around the translational gears to seal the openings (**Fig. S1**).

The cell culture chamber was designed to be biocompatible. And during the experiment, it was properly closed to create a contamination-free environment. The chamber could be opened from the top and the bottom (**Fig. S1**). We designed a removable lid to cover the top of the chamber, and small gaps were left to access air. On the bottom, an opening was made below the cell culture sample, which was sealed with a removable acrylic sheet by screws.

bioRxiv preprint doi: https://doi.org/10.1101/2021.07.07.451494; this version posted July 9, 2021. The copyright holder for this preprint (which was not certified by peer review) is the author/funder. All rights reserved. No reuse allowed without permission.

The double-layer membrane was fabricated with 1/32 in silicon film (Ean: 0604339345964) and PDMS membrane, sandwiched by glass slides (**Fig. 1c, Fig. S4a**). The silicone film (base layer) was cut with a laser cutter at 20% speed, 80% power, 2500 Hz frequency, 600 DPI resolution using vector job type to create the desired shape. Dow Corning Sylgard 184 silicone elastomer and cure agent (GMID: 04019862) were mixed in the 10:1 ratio to fabricate the PDMS membrane (top layer). A small amount (<300 ml) of PDMS was dropped on the center of an Ø85 mm acrylic circle. The PDMS was spin-coated the acrylic circle at 500 RPM for 30s and then at 1000 RPM for another 2 mins (WS650MZ23NPPB, Laurell Technologies). We then cured the PDMS-coated acrylic circle at a 65 C° oven overnight. A thin layer of PDMS membrane with a thickness of around 100μm was formed on top of the acrylic circle. The thickness was measured with a precise micrometer (293-340330, Mitutoyo). The PDMS coated acrylic was laser cut into the 22×14 mm rectangle shape for the triangle sample and the 14×14 mm square shape for the square sample (**Fig. 1c**). The glass slide (125444, Fisher Scientific) was cut into 20×25 mm pieces. We laser printed acrylic modes in the shape of the cell culture sample for precise alignment (**Fig. S4**). To cut through the acrylic, we used 100% power and 10% speed. To cut marks on top of the mode, we used 20% power and 50% speed. We then cleaned all parts with 100% ethanol to remove dust. The silicon film base, PDMS membrane, and glass slides were bonded with a plasma cleaner (PDC-001, Harrick plasma) at 500 psi for 3 mins, then baked at the 65 C° oven overnight. The dimensions of the sample were listed in **Fig. S6.**

REF cell culture in the cell stretching device

bioRxiv preprint doi: https://doi.org/10.1101/2021.07.07.451494; this version posted July 9, 2021. The copyright holder for this preprint (which was not certified by peer review) is the author/funder. All rights reserved. No reuse allowed without permission.

REF-52 expressed with the YFP-paxillin fusion protein (a gift from Dr. Jianping Fu) were cultured in the T-25 flask. The culture media was composed of 87% DMEM (11960051, Gibco, ThermoFisher), 10% FBS (10082147, Gibco, ThermoFisher), 1% MEM NEAA (11140050, Gibco, ThermoFisher), 1% GlutaMAX (35050061, Gibco, ThermoFisher), and 1% Penicillin-Streptomycin (15140122, Gibco, ThermoFisher). For passaging the cells, the flask was rinsed with 2 ml 1× DPBS then incubated at 37 C°, 1 ml 0.25% Trypsin-EDTA (25200072, Gibco, ThermoFisher) for 3 mins to detach the cells. 5 ml of culture media was added for dilution after cell detachment. The mixture was transferred to a 15ml tube and centrifuged at 1200 RPM for 3 mins. Then we aspirated the supernatant and resuspended the cells with 1 ml culture media. The REF cells were sub-confluent passaged at the 1:10 ratio at 1200 K cells/ml seeding density every four days.

To prepare the device for cell seeding. The double-layer membranes were first sonicated for 5 mins in 100% ethanol to remove all particles on the surface, then sterilized by autoclaving. The cell stretch device was sprayed with 70% ethanol, then dried in a biosafety cabinet. To avoid the effect of haptotaxis, we stretched the membranes to the desired magnitudes before coating fibronectin. We incubated the membranes at room temperature with 50 μg/ml fibronectin (33016-015, Gibco, ThermoFisher) by dropping 100 ml solution on the cell culture area. Then we rinsed off the fibronectin with 1× DPBS.

The cells were seeded at the density of 50 K to 80 K/ml by dropping 100 ml cell suspensions on top of the cell culture area. The device was then put into a 37 °C incubator for 1 hr to

bioRxiv preprint doi: https://doi.org/10.1101/2021.07.07.451494; this version posted July 9, 2021. The copyright holder for this preprint (which was not certified by peer review) is the author/funder. All rights reserved. No reuse allowed without permission.

facilitate cell attachment, and then 5 ml culture media was added. The cells were left overnight to attach fully. The stretching and imaging procedure would begin 15 hrs after cell seeding. Before cell tracking, we would draw lines on the image sequence to encircle the region for cell tracking (**Fig. 2a**). All cells with clear migration trajectories within the encircled region were tracked with the ImageJ MTrackJ plugin.

Ansys Simulation of the Strain field

Finite element modeling of the cell culture samples was conducted using the Ansys simulation software. Two-layer 3-D models were constructed to mimic the structures of the cell culture sample (**Fig. S7a**). The PDMS membrane was defined to bond on top of the silicone base (**Fig. S7b**). For simplicity, only the center parts of the stretched regions were modeled. For the silicone film, a tensile test was conducted to acquire the test stress-strain data (Mark-10 Force Gauge Model M7-5), which was curve-fitted using the polynomial 2nd order equation in the simulation (**Fig. S7c**). For the PDMS membrane, the material properties were defined based on previous literature (45), with Young's modulus set to 1.1 MPa, the Poisson's ratio to 0.45, and density to 970 kg/m^3.

In the simulation, the forces applied in the x-direction were estimated to conform to the experimental strain magnitude across the cell culture area. To mimic the uniaxial stretching, forces were applied on both sides of the models (**Fig. S7a**). The setups of the simulation were described in **Table S1**.

bioRxiv preprint doi: https://doi.org/10.1101/2021.07.07.451494; this version posted July 9, 2021. The copyright holder for this preprint (which was not certified by peer review) is the author/funder. All rights reserved. No reuse allowed without permission.

Strain field calibration

To quantify the strain across the cell culture area, small markers (Ø 50 μm) with equal distance were printed using the micro-contact printing technique. Two types of micro-contact printing patterns were applied, one with a distance of 100 μm, and the other with a distance of 80 μm between the center of two adjacent markers. The traditional photolithography method was adopted to fabricate the PDMS stamp (46). We incubated the PDMS stamp with the 50 μg/ml Alexa Fluor 555-labeled BSA (A34786, Molecular Probes) at room temperature for 1 hr. Then the stamp was rinsed with DI water and blow-dried. The membranes were UV treated for 7 mins for surface activation (30, Jelight Company). The fluorescence makers were printed by pressing the PDMS stamp onto the membrane.

The strain was calculated by quantifying the change of distance between two adjacent markers in the stretch direction (**Fig. S2**). The strain field was mapped based on the coordinates of the markers after stretching and the corresponding strains using the Matlab *contourf*. For each sample, the strain field was symmetrical based on the x-axis starting from the triangle's vertex for the gradient triangle design. For the uniform square sample, the strain field was symmetrical both in the x and y direction to the sample's center. To reduce variations during calibration, the strain field was averaged based on the respective symmetry axes for both designs.

Three samples for both designs were calibrated (**Fig. S3**). To compare each sample's strain field, we plotted the strain magnitude against the distance from the zero coordinate in the direction L1, L2, and L3 (**Fig. S3b, d**). For the triangle design, the zero coordinate was the vertex (**Fig.**

bioRxiv preprint doi: https://doi.org/10.1101/2021.07.07.451494; this version posted July 9, 2021. The copyright holder for this preprint (which was not certified by peer review) is the author/funder. All rights reserved. No reuse allowed without permission.

S3a), and the L1 was the line starting from the vertex to the x-direction. L2 and L3 were acquired by rotating L1 for 15 and 30 degrees counterclockwise, respectively. For the square design, the zero coordinate was the square center (**Fig. S3c**), the L1 was starting from the center to the x-direction, and L2 and L3 were acquired by rotating L1 for 45 and 90 degrees counterclockwise, respectively. Data points close to the reference lines were used for quantifications (**Fig. S3a, c**). To compare the gradient, the plots were linearly fitted to acquire the slopes (**Fig. S3b, d**). Three slopes were obtained for reference lines L1 to L3 for each sample. One-way ANOVA test was used to compare individual samples using the slopes for both designs. No significant differences were found between samples.

Microscopy for cell migration trajectory

An epifluorescence microscope (Leica, DMi8) was used to image the cell migration trajectories. During the experiment, the device was kept in the 37 C° incubators for cell culturing. We placed the device onto the microscope stage outside the incubator for imaging, which would take less than 2 mins each time for each sample in the cell migration tracking experiment using the 10× phase contrast. Small air bubbles might be trapped underneath the corner of the cell culture area, which could be removed by lightly knocking the device one or two times. For the consistency of the culture condition, all samples would be subjected to the same knocking motion before imaging. The images were acquired every 50 mins for the static strain condition and every 30 mins for the cyclic strain condition for 6 hrs.

The obtained image sequences were aligned by tracking two reference points that stayed at the

bioRxiv preprint doi: https://doi.org/10.1101/2021.07.07.451494; this version posted July 9, 2021. The copyright holder for this preprint (which was not certified by peer review) is the author/funder. All rights reserved. No reuse allowed without permission.

constant location on the cell culture sample for the entire experiment period. The reference points could be small particles left on the sample surface. The first image acquired after the stretching step was set to be the fixed image. We used the Matlab *fitgeotrans* function for the translation and the *imrotate* function for the rotation to align the image sequence of cell migration. After the image sequence was aligned, the cell migration trajectories were clear to be tracked. The representative cell tracking movies for five experiment groups were listed in **Video S1-S5**.

Device modification for focal adhesion imaging

We adjusted the designs of the device to allow high-resolution imaging for focal adhesion analysis. To minimize the distance between the cells and the objective, we specifically designed a glass bottom PDMS dish (**Fig. S5**). 30g of PDMS was poured into a 60 mm Petri dish to form a dish-shaped PDMS slab. A 20×46 mm cuboid was cut off in the middle, and then the opening was covered by bonding a thin 24×50 mm cover slide using a plasma cleaner. The dish was baked in a 65 °C oven overnight for firm bonding. The removable bottom of the device was redesigned as well (**Fig. S1**). We laser cut a 60 mm diameter opening on the removable acrylic bottom. The opening was designed to hold the PDMS dish properly, and small gaps were left for manual adjustment of the height of the PDMS dish during focal adhesion imaging.

The PDMS membrane could potentially reduce the quality of the focal adhesion image. To solve this problem, we flipped the cell culture sample to make cells face down during imaging (**Fig. S5**). To fit the cell culture sample into the PDMS dish, the glass slide was cut into smaller

bioRxiv preprint doi: https://doi.org/10.1101/2021.07.07.451494; this version posted July 9, 2021. The copyright holder for this preprint (which was not certified by peer review) is the author/funder. All rights reserved. No reuse allowed without permission.

20×14 mm pieces (**Fig. S5b**). The PDMS membrane and the silicone film base were bonded at the first step. Then the sample was flipped to bond the glass slides on the opposite side of the PDMS membrane (**Fig. S5a**). The sample was baked at 65 °C in an oven overnight for firm bonding after both steps. The sample was then mounted onto the device. During the experiment, we flipped the device to coat fibronectin and seed cells. Then the device was put into the incubator upside down for cells to attach for 1 hour. We then flipped the device back and added 3 to 5ml culture media into the PDMS dish. The culture media component was adjusted by replacing the DMEM with the non-phenol red type (21063029, Gibco, ThermoFisher). Other reagents remained the same as other cell migration experiments.

Right after taking the first image, the sample was stretched once, and then the device was placed back into the incubator for 10 mins before taking the second image. The time gap between two focal adhesion images was within 20 mins. The 40× objective and YFP cube were adopted to image the focal adhesion.

Focal adhesion image processing and quantification

The focal adhesion raw images were processed through ImageJ. First, we applied the raw image with the *Subtracted Background*. Then we chose the *Sliding paraboloid* option, and the *Rolling ball radius* was set to be 50 pixels. Then we ran the *CLAHE* plugin, set the *Blocksize* equal to 19, *Histogram bins* equal to 256, and the *Maximum slope* equal to 6. Then we adjusted the *Brightness/Contrast* automatically to bright the image. The focal adhesions were enhanced at this point. We turned the image format into 8 bits and adjusted the threshold automatically. The

bioRxiv preprint doi: https://doi.org/10.1101/2021.07.07.451494; this version posted July 9, 2021. The copyright holder for this preprint (which was not certified by peer review) is the author/funder. All rights reserved. No reuse allowed without permission.

sizes and the coordinates of focal adhesions were quantified with the *Analysis particle* option.

A variation of the image quality decline was found after the stretching, which would make the size of focal adhesion inaccurate to be quantified for the second image. Therefore, to effectively compare the focal adhesion size change within each cell, the data was normalized using images prior to stretching. The normalization was calculated as below:

$$P_H^N = \frac{A_{H2} \times \frac{A_1}{A_2} - A_{H1}}{A_{H1}}$$

A_1, A_{H1} : The focal adhesion size for the entire and one half of the cell before stretching, respectively.

A_2 , A_{H2}: The focal adhesion size for the entire and one half of the cell after stretching, respectively.

P_H^N : Normalized percentage change of focal adhesion size the respective half of the cell.

Statistics

Statistical analysis was performed using OriginLab and R. Rayleigh tests were run to determine the unimodal distribution of circular data in cell migration direction analysis. For non-circular datasets, normality tests were run to determine the normality of the distribution. For statistical comparisons of two normal distributed datasets, P-values were calculated using the two-sample t-test. For statistical comparisons of two non-normal distributed datasets, P-values were calculated using the non-parametric Mann-Whitney test. For statistical comparisons of multiple normal distributed datasets, P-values were calculated using the one-way ANOVA test.

bioRxiv preprint doi: https://doi.org/10.1101/2021.07.07.451494; this version posted July 9, 2021. The copyright holder for this preprint (which was not certified by peer review) is the author/funder. All rights reserved. No reuse allowed without permission.

ACKNOWLEDGMENT

This work is supported in part by the National Science Foundation (CMMI 1662835 and CMMI 1846866 to Y.S.).

AUTHOR CONTRIBUTIONS

F. Y. designed and performed all the experiments, analyzed the data, and wrote the manuscript.

Y. S. supervised the project and edited the manuscript.

DECLARATION OF INTERESTS

The authors declare no competing interests.

bioRxiv preprint doi: https://doi.org/10.1101/2021.07.07.451494; this version posted July 9, 2021. The copyright holder for this preprint (which was not certified by peer review) is the author/funder. All rights reserved. No reuse allowed without permission.

FIGURES

Figure 1

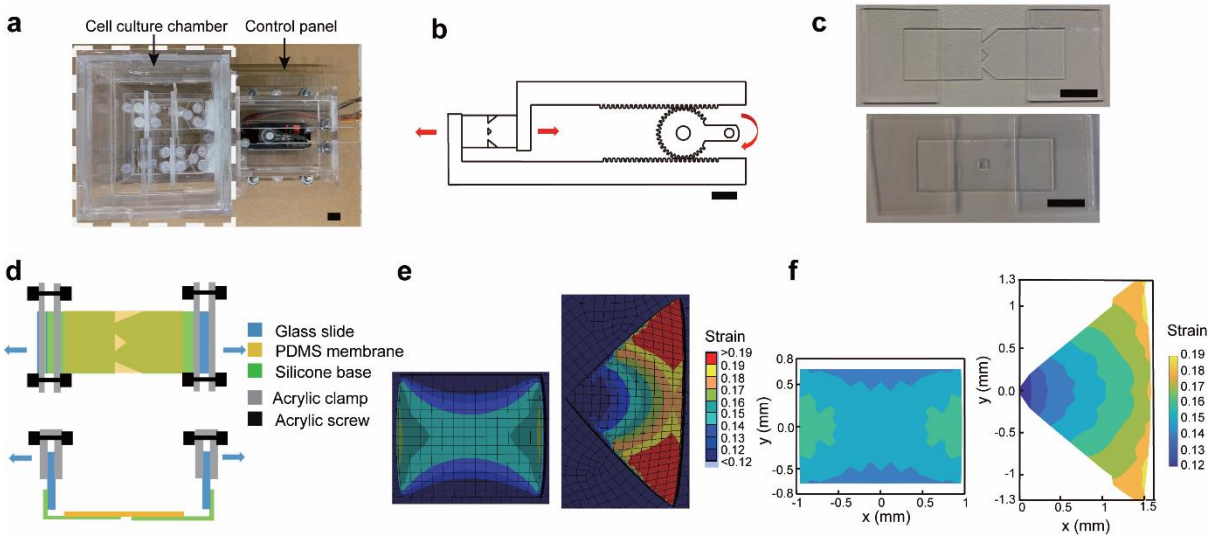

Fig 1. Design and calibration of the strain gradient generation device. **(a)** Photo of the strain gradient generation device. Scale bar, 10 mm. **(b)** Drawing of the gear control mechanism. Scale bar, 10 mm. **(c)** Photo of membranes with triangle cut-out (top) and square cut-out (bottom). Scale bar, 10 mm. **(d)** Schematic showing device assembly and stretching application. **(e)** Simulated strain fields for uniform strain (left) and strain gradient (right). **(f)** Strain map showing experimental calibration of strain fields for uniform strain (left) and strain gradient (right).

bioRxiv preprint doi: https://doi.org/10.1101/2021.07.07.451494; this version posted July 9, 2021. The copyright holder for this preprint (which was not certified by peer review) is the author/funder. All rights reserved. No reuse allowed without permission.

Figure 2

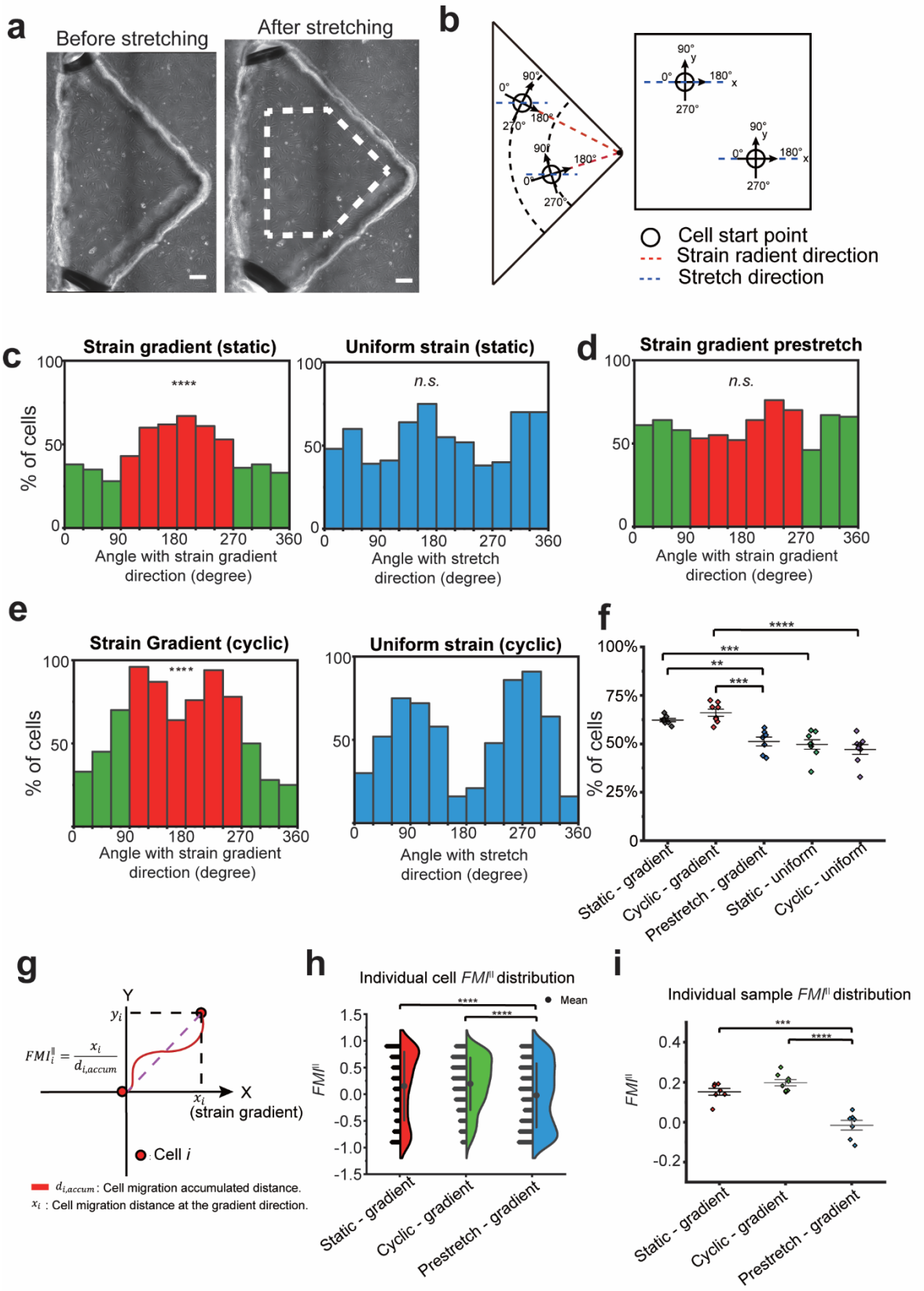

bioRxiv preprint doi: https://doi.org/10.1101/2021.07.07.451494; this version posted July 9, 2021. The copyright holder for this preprint (which was not certified by peer review) is the author/funder. All rights reserved. No reuse allowed without permission.

Fig 2. Tensotaxis behavior of REF. (a) Photos of REF seeding on the gradient cell culture sample, before (left) and after (right) stretching. Region of interests was encircled with white dash line. Scale bar, 200μm. **(b)** Schematics for the adjusted reference based on the cell's location on the gradient cell culture sample (left) and the uniform cell culture sample (right). **(c-e)** Histogram showing cell migration direction distribution under static strain gradient (**c**, left, N = 7, M = 554), uniform strain (**c**, right, N = 8, M = 654), pre-stretched static strain gradient (**d**, N = 7, M = 732), cyclic strain gradient (**e**, left, N = 8, M = 746), and cyclic uniform strain (**e**, right, N = 8, M = 630). **(f)** Individual sample's percentage of cell migrate to lower strain direction. Two sample t-tests were run between each pair of groups. **(g)** Schematic showing the $FMI^{||}$ calculation. **(h)** Individual cell's $FMI^{||}$ distribution for static gradient group (N = 7, M = 554), cyclic gradient group (N = 8, M = 746), and pre-stretched strain gradient group (N = 7, M = 732). Mann-Whitney tests were run between each pair of groups. **(i)** Individual samples' average $FMI^{||}$ distribution for static gradient group (N = 7), cyclic gradient group (N = 8), and pre-stretched strain gradient group (N = 7). Two sample t-tests were run between each pair of groups. Rayleigh tests were run to determine the unimodal distribution of the circular data. **, $P < 0.01$. ***, $P < 0.001$. ****, $P < 0.0001$. N: Sample number; M: Cell number.

bioRxiv preprint doi: https://doi.org/10.1101/2021.07.07.451494; this version posted July 9, 2021. The copyright holder for this preprint (which was not certified by peer review) is the author/funder. All rights reserved. No reuse allowed without permission.

Figure 3

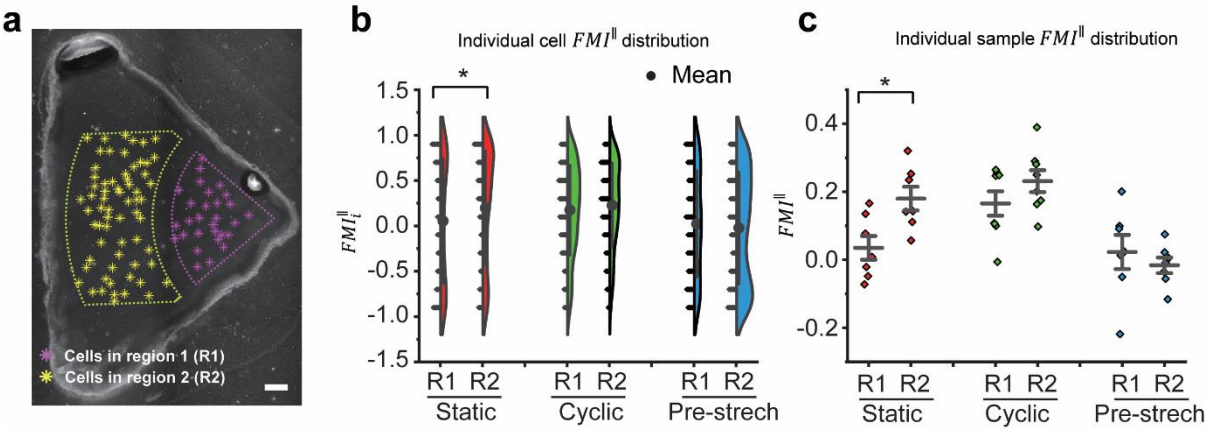

Fig 3. **Strain magnitude regulates REF tensotaxis. (a)** Photo of dividing an individual gradient sample into two strain magnitude regions. Scale bar: 200 μm. (**b**) Individual cell's $FMI^{||}$ distribution at region 1 and region 2 for the static gradient group ($N = 7$, $M1 = 180$, $M2 = 281$); cyclic gradient group ($N = 8$, $M1 = 333$, $M2 = 261$); pre-stretched static strain gradient group ($N = 7$, $M1 = 185$, $M2 = 426$). Mann-Whitney test were run between each pair of groups. (**c**) Individual samples' average $FMI^{||}$ distribution for region 1 and region 2 for the static gradient group ($N = 7$); cyclic gradient group ($N = 8$); pre-stretched static strain gradient group ($N = 7$). Two sample t-test were run between each pair of groups. *, $P < 0.05$. ***, $P < 0.001$. ****, $P < 0.0001$. N: Sample number; $M1$: Cell quantity in region 1; $M2$: Cell quantity in region 2.

bioRxiv preprint doi: https://doi.org/10.1101/2021.07.07.451494; this version posted July 9, 2021. The copyright holder for this preprint (which was not certified by peer review) is the author/funder. All rights reserved. No reuse allowed without permission.

Figure 4

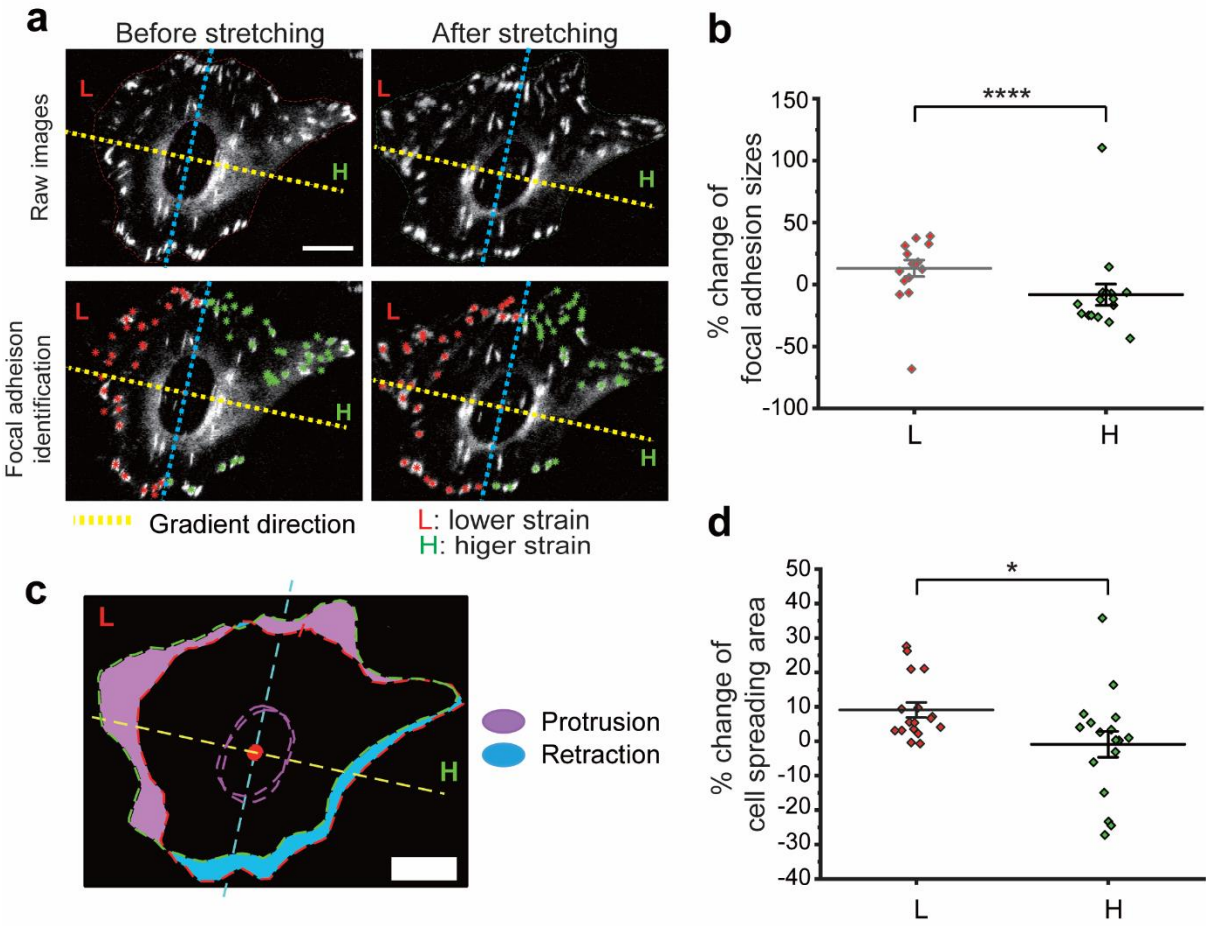

Fig 4. Focal adhesion dynamics and polarized cell protrusion in response to strain gradient. (a) Raw images (top) and processed images (bottom) of a representative REF cell with focal adhesions identified before (left) and after (right) stretching. Scale bar 20 μm. Focal adhesions that were analyzed before (up) and after (down) stretching under a static strain gradient. Scale bar, 20 μm. **(b)** Normalized percentage change of the total focal adhesion area in the lower and higher strain half (N = 16). **(c)** Overlapping the images before and after stretching. The protrusions and retractions after stretching were color coded. **(d)** Percentage of cell area change in the lower and higher strain half (N = 17). Two sample t-test were run. *, $P < 0.05$. ****, $P < 0.0001$. N: cell quantity.

bioRxiv preprint doi: https://doi.org/10.1101/2021.07.07.451494; this version posted July 9, 2021. The copyright holder for this preprint (which was not certified by peer review) is the author/funder. All rights reserved. No reuse allowed without permission.

REFERENCES

1. Ayad NME, Kaushik S, & Weaver VM (2019) Tissue mechanics, an important regulator of development and disease. *Philos Trans R Soc Lond B Biol Sci* 374(1779):20180215.
2. Swartz MA & Fleury ME (2007) Interstitial flow and its effects in soft tissues. *Annu Rev Biomed Eng* 9:229-256.
3. Sun Y, Chen CS, & Fu J (2012) Forcing stem cells to behave: a biophysical perspective of the cellular microenvironment. *Annual Review of Biophysics* 41:519-542.
4. Abilez OJ*, et al.* (2018) Passive Stretch Induces Structural and Functional Maturation of Engineered Heart Muscle as Predicted by Computational Modeling. *Stem cells (Dayton, Ohio)* 36(2):265-277.
5. Gudipaty SA*, et al.* (2017) Mechanical stretch triggers rapid epithelial cell division through Piezo1. *Nature* 543(7643):118-+.
6. Beloussov LV, Louchinskaia NN, & Stein AA (2000) Tension-dependent collective cell movements in the early gastrula ectoderm of Xenopus laevis embryos. *Dev Genes Evol* 210(2):92-104.
7. Wang H, Ip W, Boissy R, & Grood ES (1995) Cell orientation response to cyclically deformed substrates: experimental validation of a cell model. *J Biomech* 28(12):1543-1552.
8. Abiko H*, et al.* (2015) Rho guanine nucleotide exchange factors involved in cyclic-stretch-induced reorientation of vascular endothelial cells. *Journal of Cell Science* 128(9):1683-1695.
9. Livne A, Bouchbinder E, & Geiger B (2014) Cell reorientation under cyclic stretching. *Nature Communications* 5(1):3938.
10. Serwane F*, et al.* (2017) In vivo quantification of spatially varying mechanical properties in developing tissues. *Nat Methods* 14(2):181-186.
11. von Dassow M & Davidson LA (2009) Natural Variation in Embryo Mechanics: Gastrulation in Xenopus laevis Is Highly Robust to Variation in Tissue Stiffness. *Developmental Dynamics* 238(1):2-18.
12. Reig G*, et al.* (2017) Extra-embryonic tissue spreading directs early embryo morphogenesis in killifish. *Nature Communications* 8(1):15431.
13. Márquez S, Reig G, Concha M, & Soto R (2019) Cell migration driven by substrate deformation gradients. *Physical Biology* 16(6):066001.
14. Van Haastert PJ & Devreotes PN (2004) Chemotaxis: signalling the way forward. *Nat Rev Mol Cell Biol* 5(8):626-634.
15. Carter SB (1967) Haptotaxis and the mechanism of cell motility. *Nature* 213(5073):256-260.
16. Ricoult SG, Kennedy TE, & Juncker D (2015) Substrate-bound protein gradients to study haptotaxis. *Front Bioeng Biotechnol* 3:40.
17. Park J, Kim DH, & Levchenko A (2018) Topotaxis: A New Mechanism of Directed Cell Migration in Topographic ECM Gradients. *Biophys J* 114(6):1257-1263.
18. Lo CM, Wang HB, Dembo M, & Wang YL (2000) Cell movement is guided by the rigidity of the substrate. *Biophys. J.* 79(1):144-152.
19. Richardson WJ, Metz RP, Moreno MR, Wilson E, & Moore JE, Jr. (2011) A device to

bioRxiv preprint doi: https://doi.org/10.1101/2021.07.07.451494; this version posted July 9, 2021. The copyright holder for this preprint (which was not certified by peer review) is the author/funder. All rights reserved. No reuse allowed without permission.

study the effects of stretch gradients on cell behavior. *J Biomech Eng* 133(10):101008.

20. Lin SL*, et al.* (2009) Effects of compressive residual stress on the morphologic changes of fibroblasts. *Med Biol Eng Comput* 47(12):1273-1279.
21. Bueno J, Bazilevs Y, Juanes R, & Gomez H (2017) Droplet motion driven by tensotaxis. *Extreme Mech Lett* 13:10-16.
22. Rosalem GS, Las Casas EB, Lima TP, & Gonzalez-Torres LA (2020) A mechanobiological model to study upstream cell migration guided by tensotaxis. *Biomech Model Mechanobiol* 19(5):1537-1549.
23. Yung YC, Vandenburgh H, & Mooney DJ (2009) Cellular strain assessment tool (CSAT): precision-controlled cyclic uniaxial tensile loading. *J Biomech* 42(2):178-182.
24. Chagnon-Lessard S, Jean-Ruel H, Godin M, & Pelling AE (2017) Cellular orientation is guided by strain gradients. *Integrative Biology* 9(7):607-618.
25. Morita Y, Sato T, Watanabe S, & Ju Y (2015) Determination of Precise Optimal Cyclic Strain for Tenogenic Differentiation of Mesenchymal Stem Cells Using a Non-uniform Deformation Field. *Experimental Mechanics* 55(3):635-640.
26. Wang L*, et al.* (2015) Patterning Cellular Alignment through Stretching Hydrogels with Programmable Strain Gradients. *ACS Applied Materials & Interfaces* 7(27):15088-15097.
27. Lu J*, et al.* (2015) Cell Orientation Gradients on an Inverse Opal Substrate. *ACS Applied Materials & Interfaces* 7(19):10091-10095.
28. Langevin HM*, et al.* (2006) Fibroblast spreading induced by connective tissue stretch involves intracellular redistribution of α- and β-actin. *Histochemistry and Cell Biology* 125(5):487-495.
29. Tremblay D, Chagnon-Lessard S, Mirzaei M, Pelling AE, & Godin M (2014) A microscale anisotropic biaxial cell stretching device for applications in mechanobiology. *Biotechnol Lett* 36(3):657-665.
30. Huh D*, et al.* (2010) Reconstituting organ-level lung functions on a chip. *Science* 328(5986):1662-1668.
31. Halldorsson S, Lucumi E, Gomez-Sjoberg R, & Fleming RMT (2015) Advantages and challenges of microfluidic cell culture in polydimethylsiloxane devices. *Biosens Bioelectron* 63:218-231.
32. Freund JB, Goetz JG, Hill KL, & Vermot J (2012) Fluid flows and forces in development: functions, features and biophysical principles. *Development* 139(7):1229-1245.
33. Johnston ID, McCluskey DK, Tan CKL, & Tracey MC (2014) Mechanical characterization of bulk Sylgard 184 for microfluidics and microengineering. *J Micromech Microeng* 24(3).
34. Liu M, Sun J, Sun Y, Bock C, & Chen Q (2009) Thickness-dependent mechanical properties of polydimethylsiloxane membranes. *J Micromech Microeng* 19(3):035028.
35. Geiger B & Yamada KM (2011) Molecular architecture and function of matrix adhesions. *Cold Spring Harb Perspect Biol* 3(5).
36. Foxman EF, Kunkel EJ, & Butcher EC (1999) Integrating conflicting chemotactic signals. The role of memory in leukocyte navigation. *The Journal of cell biology* 147(3):577-588.

bioRxiv preprint doi: https://doi.org/10.1101/2021.07.07.451494; this version posted July 9, 2021. The copyright holder for this preprint (which was not certified by peer review) is the author/funder. All rights reserved. No reuse allowed without permission.

37. Malet-Engra G, *et al.* (2015) Collective cell motility promotes chemotactic prowess and resistance to chemorepulsion. *Curr Biol* 25(2):242-250.
38. DuChez BJ, Doyle AD, Dimitriadis EK, & Yamada KM (2019) Durotaxis by Human Cancer Cells. *Biophys J* 116(4):670-683.
39. Trepat X, Chen Z, & Jacobson K (2012) Cell migration. *Comprehensive Physiology* 2(4):2369-2392.
40. Weng S, Shao Y, Chen W, & Fu J (2016) Mechanosensitive subcellular rheostasis drives emergent single-cell mechanical homeostasis. *Nat Mater*.
41. Plotnikov Sergey V, Pasapera Ana M, Sabass B, & Waterman Clare M (2012) Force Fluctuations within Focal Adhesions Mediate ECM-Rigidity Sensing to Guide Directed Cell Migration. *Cell* 151(7):1513-1527.
42. Wormer DB, Davis KA, Henderson JH, & Turner CE (2014) The Focal Adhesion-Localized CdGAP Regulates Matrix Rigidity Sensing and Durotaxis. *PLOS ONE* 9(3):e91815.
43. Wong S, Guo W-H, & Wang Y-L (2014) Fibroblasts probe substrate rigidity with filopodia extensions before occupying an area. *Proceedings of the National Academy of Sciences* 111(48):17176-17181.
44. Raab M, *et al.* (2012) Crawling from soft to stiff matrix polarizes the cytoskeleton and phosphoregulates myosin-II heavy chain. *Journal of Cell Biology* 199(4):669-683.
45. Dinh THN, Martincic E, Dufour-Gergam E, & Joubert PY (2017) Mechanical Characterization of PDMS Films for the Optimization of Polymer Based Flexible Capacitive Pressure Microsensors. *Journal of Sensors* 2017:8235729.
46. Qin D, Xia Y, & Whitesides GM (2010) Soft lithography for micro- and nanoscale patterning. *Nature Protocols* 5(3):491-502.